Polarization and hyperfine transitions of metastable ^{129}Xe in discharge cells

T. Xia, S. W. Morgan, Y.-Y. Jau, and W. Happer
Department of Physics, Princeton University, Princeton, New Jersey 08544, USA
(Received 9 June 2009; published 22 March 2010)

The polarization and relaxation rates of metastable ^{129}Xe atoms are measured with magnetic resonance spectroscopy, at both microwave frequencies, where $\Delta F = 1$ transitions are induced between the sublevels, and at radiofrequencies, corresponding to $\Delta F = 0$ transitions. The nuclear spin polarization of the resonant velocity group is measured to be $22 \pm 2\%$. The relaxation of metastable xenon atoms is dominated by depolarizing collisions with ground-state atoms, with lesser contributions from metastability exchange collisions.

DOI: 10.1103/PhysRevA.81.033419 PACS number(s): 32.80.Xx, 32.30.Dx, 52.80.Pi, 32.30.Bv

I. INTRODUCTION

Spin-polarized metastable helium [1] produced by optical pumping of helium gas in a weak electric discharge has been used in atomic magnetometers [2] and is also used to polarize ^{3}He nuclei of ground-state atoms [3]. The metastable states of neon, argon, and xenon have also been optically pumped [4,5], but so far experiments aimed at polarizing the nuclei of heavier noble gases by optical pumping of the metastable states have not been very successful. The principal original purpose of this experiment was to examine the use of metastable ^{129}Xe to make an atomic clock. The observation of the hyperfine resonance has been done. However, the results show that our experimental conditions do not make a good candidate for an atomic clock. The work described in this article was also undertaken in part to learn more about the prospects of using metastable pumping to produce spin-polarized nuclei of the heavier noble gases.

In the case of xenon [5–8], most previous optical-pumping experiments have used the $1s_5 \rightarrow 2p_8$ transition (Paschen notation [9]). Data from these experiments indicate that the Zeeman magnetic resonance linewidths are ≈30–60 kHz full width at half maximum (FWHM) at 10 mTorr Xe pressure in even isotopes of Xe. Studies of $\Delta F = 0$ radiofrequency (rf) resonances for the the $F = 5/2$ and $F = 3/2$ of metastable ^{129}Xe ($I = 1/2$) have been reported by [6]. Measurements of $\Delta F = 1$ resonances in metastable noble gas atoms have been made in atomic beam experiments and at cryogenic temperatures [10–12]. Unlike earlier work, which mostly used $\Delta F = 0$ rf resonances for monitoring spin polarization of even isotopes of the metastable atoms, the work reported here was focused on the isotope ^{129}Xe, where we used both $\Delta F = 0$ rf resonances and $\Delta F = 1$ microwave resonances. This permits us to more unambiguously determine the degree of nuclear spin polarization of the optically pumped metastable atoms. In the experiments discussed in this article, we usually pumped to the $2p_6$ level, rather than the $2p_8$ level most commonly used in earlier work.

Table I lists useful properties of the metastable and excited states of Xe for these experiments. The electronic configuration of metastable xenon consists of tightly bound core electrons in the first five shells with an electron hole in a $5p_{1/2}$ or $5p_{3/2}$ shell and a "valence" electron in the s orbital of the next unoccupied shell, $6s_{1/2}$. There are different possible couplings of the angular momenta of the core and valence electrons. We denote the coupled state as $[5p_j, 6s_{1/2}]_J$. The possible couplings are $[5p_{1/2}, 6s_{1/2}]_0$, $[5p_{1/2}, 6s_{1/2}]_1$, $[5p_{3/2}, 6s_{1/2}]_1$, and $[5p_{3/2}, 6s_{1/2}]_2$. In these experiments, we will refer to the state with $J = 2$ as "the metastable state." Neither the state with $J = 2$ nor the state with $J = 0$ from the configuration $5p^5 6s$ can make electric-dipole transitions to the ground state with $J = 0$ from the configuration $5p^6$ because of the selection rule $\Delta J = 0, 1$, but $J = 0 \rightarrow J = 0$ is forbidden. Metastable xenon can be optically pumped into a higher excited state by near-IR photons from a laser or lamp that excite the $6s$ valence electron to a $6p$ excited state (see Fig. 1).

II. EXPERIMENT

A sketch of the experimental apparatus is shown in Fig. 2. The metastable $1s_5$ state of Xe (enriched to 86% ^{129}Xe) is populated with a weak electrical discharge driven by external electrodes at a frequency of approximately 100 MHz. The Pyrex cell used for the optical absorption measurements has a Xe pressure of 1 Torr, and the cell used for the magnetic resonance experiments has a Xe pressure of $\lesssim$12 mTorr. The metastable Xe density for the magnetic resonance experiments is determined by measuring the optical attenuation of the laser at intensities small enough to avoid saturation of the optical transition or optical pumping of the spins of the metastable atoms. The measured metastable Xe density for the $1s_5$ level is $\approx 10^{11}$ atoms cm^{-3} and varies slightly with pressure (see Fig. 3), while the total Xe density is $\approx 10^{14}$ cm^{-3}. The metastable state can be pumped to one of the $2p$ excited states (see Table I). The lasers used include a Ti:sapphire laser for the optical absorption measurements and a Toptica diode laser for the magnetic resonance experiments. Circularly polarized light is normally used to pump the atoms into end states. A microwave field is applied to induce $\Delta F = \pm 1$ transitions between the hyperfine sublevels, and we observe the change in light transmission as the microwave field is swept through resonance conditions. The microwave field is amplitude-modulated at a low frequency (3.3 kHz) and the light transmission is monitored using a lock-in amplifier. The linewidths, typically ∼100 kHz, are strongly influenced by the light intensity, the microwave intensity, and collisions with other atoms as well as with the walls of the container. By using rf instead of microwaves, we also studied $\Delta F = 0$ Zeeman transitions.

Previous reports [3,6] have noted that the discharge can drive impurities or noble gas atoms either into or out of

TABLE I. Some useful properties of metastable and excited states in Xe. The metastable level is $1s_5$ (Paschen notation). The oscillator strengths are averages of theoretically estimated length and velocity oscillator strengths.

Energy level (Paschen notation)	$1s_5$	$2p_6$	$2p_7$	$2p_8$	$2p_9$	$2p_{10}$
Energy level (Racah notation)	$6s[\frac{3}{2}]_2$	$6p[\frac{3}{2}]_2$	$6p[\frac{3}{2}]_1$	$6p[\frac{5}{2}]_3$	$6p[\frac{5}{2}]_2$	$6p[\frac{1}{2}]_1$
Electronic angular momentum J	2	2	1	3	2	1
Landé factor g_J	1.5	1.378	1.024	1.333	1.106	1.853
Excitation λ from $1s_5$ level (nm) [9]		823.4	841.1	882.2	904.8	980.2
Hyperfine constant A for ^{129}Xe (MHz) [10,13–15]	−2384.4	−889.6	−1310.6	−873.2	−1364.2	−1401.7
Oscillator strength f from $1s_5$ level [16]		0.24	0.013	0.56	0.12	0.24

the walls of the cell. We also noticed that after some short period of time (on the order of hours or days), the optical absorption properties as well as the color of the discharge in the cells changed. Because the cells had been baked to 350°C prior to filling them, the changes were not due simply to outgassing, but to the discharge. Even by plasma cleaning our cells we were unsuccessful at eliminating this problem of contamination. This may partially be due to the low-compression-ratio turbomolecular pumps such as ours have for hydrogen. By discharging a low-pressure (several mTorr) cell on the vacuum system and using a residual gas analyzer (RGA), we found that hydrogen was being driven off the walls during discharge, as well as smaller amounts of water and nitrogen. These molecules easily attach free electrons and make it harder to maintain the discharge. Because of this, we obtained small Zr-V-Fe alloy getters [17] to absorb the hydrogen, water, and nitrogen. These getters were successful in eliminating hydrogen, water, and nitrogen when activated (see Fig. 4), and the properties of the cell were observed to remain constant for the duration of the measurements. The getters are slightly magnetic, so they were kept away from the portion of the cell that was excited. In order to prevent Xe atoms driven to and from the walls from changing the pressure, we use a liquid nitrogen cryotrap to pump most of the Xe atoms out of the discharge volume and to allow the vapor pressure to maintain constant Xe density in our cell. A capacitance manometer is used to monitor the cell pressure, and the temperature of the cryotrap is controlled to change the vapor pressure of Xe in the cell. The excited Xe atoms are far from the cryotrap (see Fig. 2).

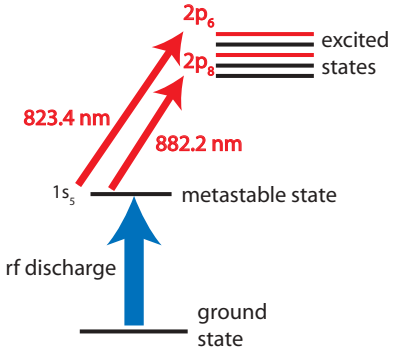

FIG. 1. (Color online) Xenon energy levels of the states involved in these experiments. The rf discharge populates the $1s_5$ metastable state, which has electronic angular momentum $J = 2$. Laser light at 823 or 882 nm excites transitions to the $2p_6$ or $2p_8$ excited states, which have $J = 2$ and $J = 3$, respectively (see also Table I).

III. RESULTS AND DISCUSSION

A. Optical spectroscopy

We acquire the optical resonance spectrum by sweeping the laser frequency through the optical transitions (see Figs. 5 and 6). A Voigt profile [18] is used to fit the optical resonances. The absorption lines have a Gaussian contribution of 400 MHz, due to Doppler broadening, and a Lorentzian contribution, due to collisions and spontaneous decay, of 110 MHz. Because the linewidth (<50 MHz) of the Ti:sapphire laser is small compared to both components of the width, metastable atoms with velocities that Doppler shift the absorption frequencies into resonance with the laser are selectively excited. The hyperfine splitting of both the metastable and the optically excited states is resolved. The measured hyperfine structure coefficients are $A_{1s_5} = -2384.4 \pm 15.8$ MHz, $A_{2p_6} = -889.6 \pm 7.9$ MHz, and $A_{2p_8} = -873.2 \pm 10.7$ MHz, in agreement with the previously reported values [10,13–15].

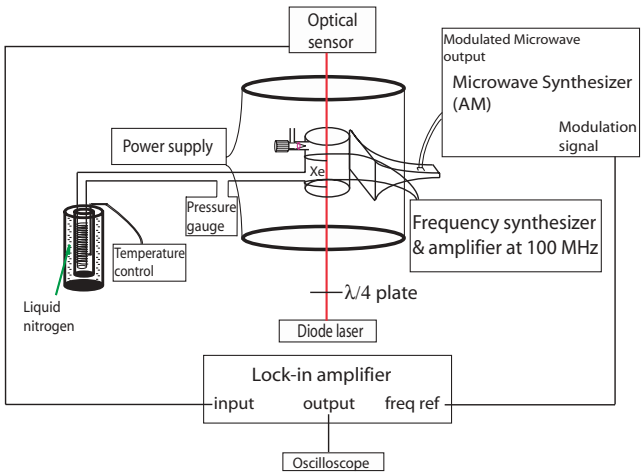

FIG. 2. (Color online) A sketch of the experimental apparatus. Xenon gas is cryopumped to a pressure of a few mTorr. An rf discharge populates the metastable state. A diode laser optically pumps the metastable Xe atoms and microwaves (rf) applied to the cell at the hyperfine (Zeeman) frequency from the microwave horn (coil) are amplitude modulated at 3.3 kHz. The microwave (rf) frequency is swept through the hyperfine (Zeeman) resonance and the change in transmission is monitored by a photodiode.

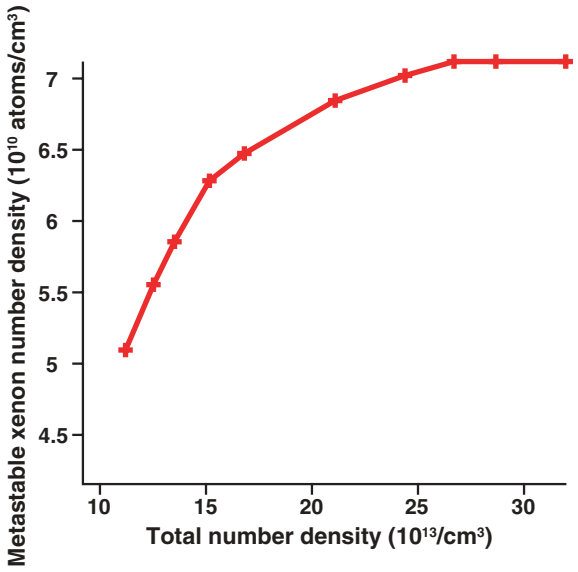

FIG. 3. (Color online) The measured density of metastable Xe atoms in the $1s_5$ level vs the measured total number density measured using a capacitance manometer. The total number density is about three orders of magnitude larger than the metastable number density.

B. Atomic and nuclear polarization of metastable ^{129}Xe

Right-circularly polarized light of wavelength 823.4 nm is tuned to maximize the transition rate from the multiplet with $F = 5/2$ of the metastable state to the multiplet with $F = 5/2$ of the $2p_6$ excited state, as shown in Fig. 5. Metastable atoms in the "dark sublevel," $|F = 5/2, m_F = 5/2\rangle$, cannot absorb this light, so optical pumping and spin relaxation enhance the population of this sublevel and neighboring sublevels with nearly the same angular-momentum quantum numbers, as shown in Fig. 7. The spin-polarized atoms are depolarized by relaxation mechanisms such as wall relaxation and collisions with ground-state Xe atoms.

Figure 8 shows a typical rf resonance, corresponding to Zeeman resonance for metastable atoms in the multiplet with $F = 3/2$ in a longitudinal field of approximately 2 G. Figure 9 shows an absorption spectrum when microwaves are applied at the hyperfine resonance frequency. The details of this spectrum

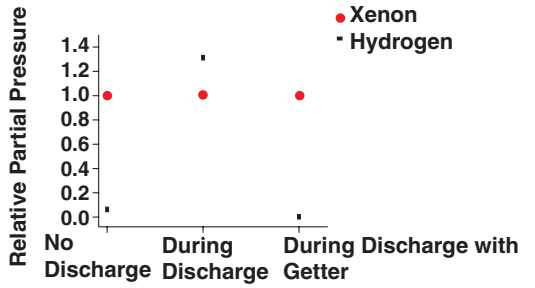

FIG. 4. (Color online) The relative partial pressures of molecular hydrogen (H_2) and ^{129}Xe measured on our RGA before and during discharge, and during discharge with a hydrogen getter inside the cell. The RGA used is able to distinguish mass-to-charge ratios to within 1 amu/electron charge. To a lesser extent, we also measured water and nitrogen contaminants in the cells. Using the hydrogen getter also reduced these contaminants.

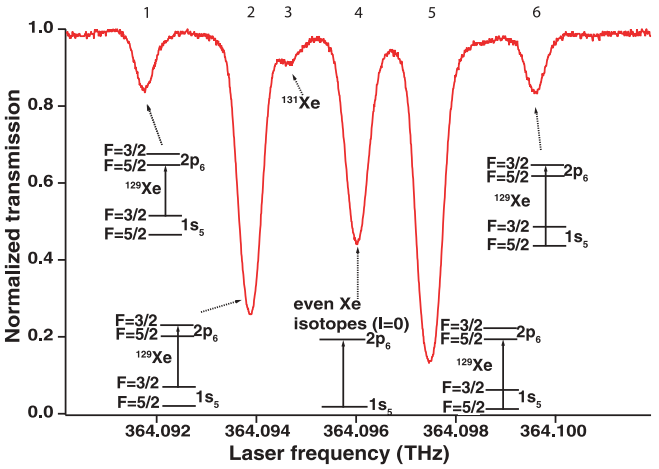

FIG. 5. (Color online) Transmission spectrum of metastable xenon at 823 nm optical excitation shows four resonances of ^{129}Xe. The isotope shift for xenon is less than the absorption linewidth, so the absorption lines from the even isotopes converge to the same peak. A small resonance of ^{131}Xe is also visible.

depend on the applied magnetic field B, how the atoms are distributed between the sublevels of the metastable state, the light intensity, and the power of the microwaves beamed onto the cell. In this spectrum, there are eight resonances in a 35-MHz interval, centered at the 5961-MHz hyperfine frequency. The longitudinal field is approximately 4.55 G. The eight resonances mainly correspond to the eight permitted σ transitions between the hyperfine multiplets $F = 3/2$ and $F = 5/2$. It was not possible to completely eliminate π transitions, which have the same frequencies as four of the σ transitions, and which slightly perturb the spectrum, as we discuss in more detail later in this article. The quantity simulated in Fig. 9 is the specific absorption of metastable ^{129}Xe atoms, that is, the ratio of the absorption rate of a polarized atom to that of a completely unpolarized atom.

In the absence of any magnetic field, the energies of the sublevels $|F, m_F\rangle$ depend only on F. Then the resonant

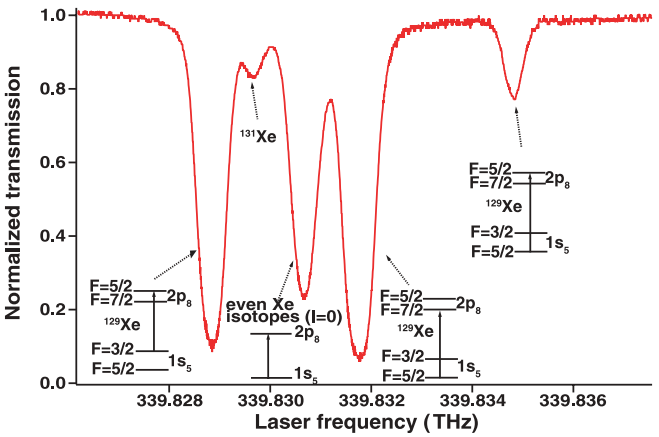

FIG. 6. (Color online) Transmission spectrum of metastable xenon at 882 nm optical excitation shows three resonances of ^{129}Xe, a converged resonance of even isotopes, and a small resonance of ^{131}Xe. All of the transitions obey the selection rule $\Delta F = 0, \pm 1$.

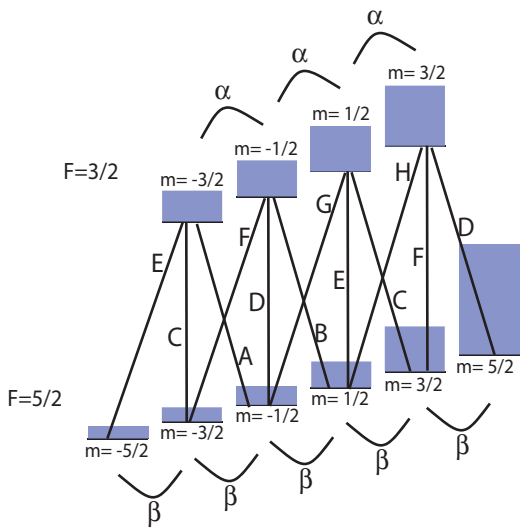

FIG. 7. (Color online) An illustration of the population distribution when metastable ^{129}Xe atoms are optically pumped. The relative populations are indicated by the heights of the vertical bars, which do not follow a spin-temperature distribution. The eight labeled crossing lines correspond to the σ hyperfine resonances in Fig. 9. The four vertical lines correspond to the π hyperfine resonances in Fig. 9. The three arc lines labeled α correspond to the Zeeman resonances in Fig. 8.

frequency for a transition from a sublevel with $F = 5/2$ to a sublevel with $F = 3/2$ is approximately $\nu_0 = 5A/(2h) =$ 5961 MHz. For the magnetic fields B on the order of a few gauss that we used in our experiments, the field-induced energy

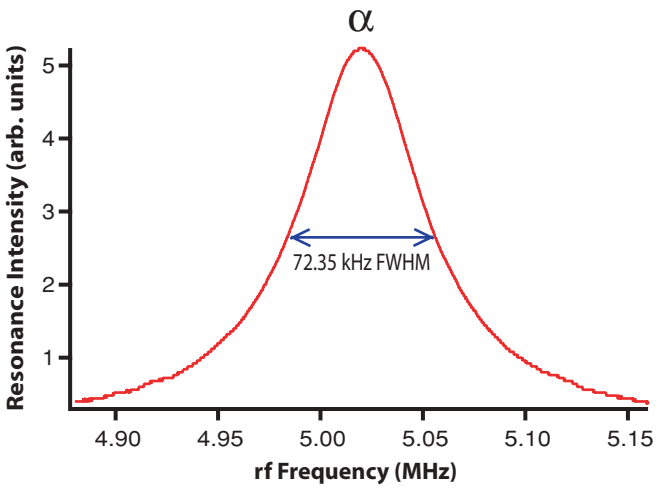

FIG. 8. (Color online) Measured optical transmission spectrum which reflects the change of the specific absorption at a fixed longitudinal magnetic field when the rf frequency is swept about the Zeeman resonance of the $F = 3/2$ hyperfine levels. At the low applied field of 2 G, different Zeeman resonances are separated by ≈240 Hz, which is the quadratic correction to the result of (1), and are not resolvable in the measurement. The Zeeman resonances are separated by ≈72 kHz at 35 G, out of range of the Helmholtz coils used.

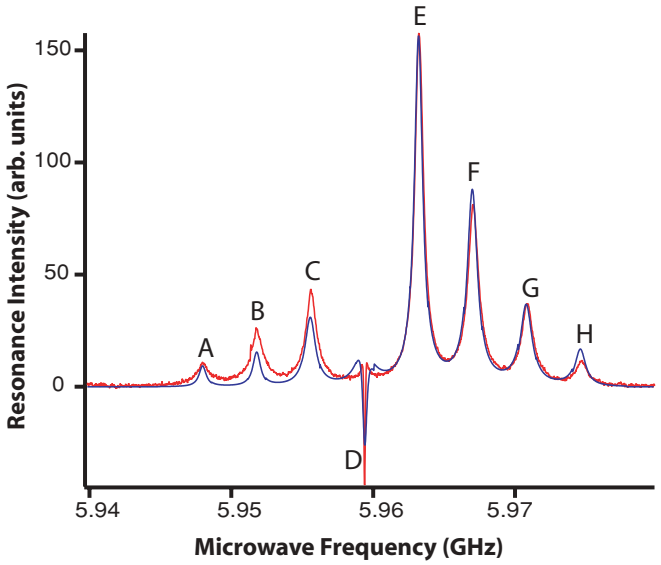

FIG. 9. (Color online) Measured (red) and simulated (blue) optical transmission spectra. The optical transmission spectrum reflects the change of the specific absorption at a fixed longitudinal magnetic field of 4.55 G when the microwave frequency is swept about the hyperfine frequency. The simulation of the ten Zeeman states' populations gives 22 ± 2% nuclear polarization and 30 ± 4% atomic polarization in the metastable state. Eight resonant components correspond to the straight transition lines in Fig. 7.

shift of the sublevel $|F, m_F\rangle$ is very nearly

$$\Delta E_{Fm_F} = g_F \mu_B B m_F, \quad \text{where}$$
$$g_F = \frac{F(F+1) + J(J+1) - I(I+1)}{2F(F+1)} g_J. \qquad (1)$$

Here μ_B is the Bohr magneton and $g_J = 1.5$ was given in Table I. We ignored the few-parts-per-thousand contribution to g_F from the interaction of the nuclear moment with the applied field B. From (1) we find the following values for g_F: $g_{3/2} =$ 1.8 and $g_{5/2} = 1.2$. Within a hyperfine manifold F, all $\Delta m_F =$ 1 resonances have the same frequencies, $\nu_F/B = g_F \mu_B/h$, with $\nu_{3/2}/B = 2.5193$ MHz G^{-1} and $\nu_{5/2}/B = (2/3)\nu_{3/2} =$ 1.6795 MHz G^{-1}. Hence, the low-field resonances lie nearly on top of one another and are unresolvable (Fig. 8). From these considerations we also see that the microwave resonance frequency for a transition from the sublevel $|3/2, m\rangle$ to the sublevel $|5/2, m + \rho\rangle$ is

$$\nu = 5961 \text{ MHz } + (m - 2\rho)840 \text{ kHz G}^{-1} B, \qquad (2)$$

which makes the adjacent hyperfine resonances ($\Delta F = \pm 1$) split by 840 MHz/G (Fig. 9). The arrangement of Fig. 2 is designed to excite σ transitions with $\rho = \pm 1$. However, because of misalignments and stray components of the microwave and static fields, we expect to weakly excite π transitions with $\rho = 0$. From inspection of (2) we see that the resonance frequency of the σ transition between $|3/2, m\rangle$ and $|5/2, m + \sigma\rangle$ with $\sigma = \pm 1$ is the same as the resonance frequency for the π transition between $|3/2, m - 2\sigma\rangle$ and $|5/2, m - 2\sigma\rangle$. In Fig. 9, the resonances labeled A, B, G, and H are isolated σ resonances; the resonances labeled C, D, E, and F are mostly due to σ resonances, but they have a small admixture of π resonances.

Numerical simulations show that under the conditions of our experiments the small admixture of π resonances to the σ resonances of C, E, and F broadens the resonance linewidth by about 10%. The effects are much more dramatic for the resonance D, which consists of a small positive π resonance, with a width comparable to that of all the other resonances, and corresponding to a transition between the sublevels $|3/2,-1/2\rangle$ and $|5/2,-1/2\rangle$, and an unusually narrow and negative σ resonance, corresponding to a transition between the sublevels $|3/2,3/2\rangle$ and $|5/2,5/2\rangle$. The σ resonance is unusually narrow because it has no laser power broadening. There is negligible optical pumping of atoms from the sublevel $|3/2,3/2\rangle$ because the laser is tuned to excite atoms in the metastable state $F=5/2$ hyperfine multiplet to the excited state. Since the light is right-circularly polarized, to excite an atom from the sublevel $|F,m\rangle=|5/2,5/2\rangle$ of the metastable state, it would have to produce an excited atom in the sublevel $|F,m\rangle=|5/2,7/2\rangle$, which does not exist. So atoms are not optically excited from the metastable sublevel $|5/2,5/2\rangle$. The negative sign of the resonance means that xenon atoms attenuate the laser less at the center of the resonance. This happens because the transition, in conjunction with the relaxation processes, transfers more atoms to the multiplet with $F=3/2$, which is not pumped by the laser.

The simulated spectrum in Fig. 9 corresponds to the population distribution shown in Fig. 7 when no microwave resonances are being driven. Because of the very good agreement between the simulated and measured spectrum of Fig. 9, the actual population distributions in our experiments must have been close to those of Fig. 7, which implies a polarization of the metastable ^{129}Xe nucleus of $22\pm2\%$ for the velocity groups that are optically pumped by the laser. The simulated populations are far from a spin-temperature distribution, where the populations of a sublevel of azimuthal quantum number m and spin-temperature parameter β would be proportional to $e^{\beta m}$, since the populations of levels with the same m_F in each multiplet may differ by a factor of $\approx$2. We also observe π transitions between the two levels with the same m_F in different hyperfine states, which would be impossible if there were a spin-temperature distribution.

The simulation is based on a calculation of the density matrix of metastable ^{129}Xe in steady state under the influence of light absorption, stimulated and spontaneous emission, collisional processes that depolarize or destroy metstable atoms, and magnetic resonance. Diffusion of metastable atoms to the cell walls is expected to completely destroy the metastable atom and its polarization. Collisions of the metastable atoms with each other, with ground-state Xe atoms, and with the electrons and ions of the discharge will also influence the spin polarization. We assume that analogous collisional relaxation processes affect the spin polarization of the optically excited atoms.

Our optical-pumping laser has a relatively narrow linewidth ($\lesssim$1 MHz) compared to the full, Doppler-broadened width ($\approx$392 MHz) of the optical absorption line. For spin-polarizing metastable atoms, we tune the laser to the center of the absorption line, where we most efficiently excite atoms with zero velocity along the direction of the laser beam. Spin polarization is transferred from the pumped velocity group to unpumped velocity groups by velocity-changing collisions.

TABLE II. Fit coefficients for the data in Fig. 10. In Fig. 9, the corresponding resonances are as follows: resonance E between $|F=5/2,m_F=-5/2\rangle$ and $|F=3/2,m_F=-3/2\rangle$, resonance F between $|F=5/2,m_F=-3/2\rangle$ and $|F=3/2,m_F=-1/2\rangle$, and resonance G between $|F=5/2,m_F=-1/2\rangle$ and $|F=3/2,m_F=1/2\rangle$. Resonance H between $|F=5/2,m_F=1/2\rangle$ and $|F=3/2,m_F=3/2\rangle$ is too weak to produce useful linewidth information.

Resonance	κ (10^3 s^{-1} mTorr^{-1})	η (10^3 s^{-1})
$F=5/2$ Zeeman	18.5 ± 1	77.0 ± 6.0
$F=3/2$ Zeeman	24.2 ± 1	84.8 ± 6.3
Resonance E	20.7 ± 0.3	71.6 ± 2.8
Resonance F	20.1 ± 1.3	83.3 ± 6.6
Resonance G	21.4 ± 1.9	84.2 ± 11.0
Resonance E (pump $F=5/2$)	21.0 ± 0.3	70.1 ± 2.8

If the rate of velocity-changing collisions, Γ_{vd}, is much larger than the rate of spin-changing collisions, Γ_{sd}, as is the case for optically pumped Cs in a xenon buffer gas, the spin polarization is transferred almost completely to the entire Maxwellian velocity distribution and the spin polarization of all velocity groups will be almost the same. For metstable Xe atoms, we expect Γ_{vd} to be about the same as for Cs atoms in Xe, but we expect Γ_{sd} to be much larger because of the p hole in the core of the metastable Xe atom. The efficiency with which the narrow-line optical pumping can fill the Maxwellian distribution will depend on the ratio $r=\Gamma_{sd}/\Gamma_{vd}$. For $r\ll1$, as is the case for alkali-metal atoms in a buffer gas, a narrow-line pumping light will produce the same spin polarization in the entire velocity distribution, while for $r\gg1$ the laser will only be able to produce spin polarization for atoms with resonant velocities. Using the diffusion coefficient of Cs in Xe to estimate Γ_{vd} and our own measurements of Table II to estimate Γ_{sd}, we find $r\approx20$, so we expect that we only polarized metastable atoms in the velocity group that is resonant with the laser. The measured polarization $22\pm2\%$ is the polarization of the resonant velocity group, since the width of a velocity group is $\approx$10 MHz FWHM.

Our model of metastability exchange is as follows: After the collision, the electronic configuration is exchanged between the two atoms, one of which is in the metastable state, the other in the ground state, namely,

$$^{129}\mathrm{Xe}^{*}+{}^{129}\mathrm{Xe}\longrightarrow{}^{129}\mathrm{Xe}+{}^{129}\mathrm{Xe}^{*}, \tag{3}$$

where ^{129}Xe* refers to metastable Xe atoms. We assume that the collision duration is so short ($\approx10^{-12}$ s) compared to the hyperfine evolution period ($\approx10^{-10}$ s) that the precollision nuclear spins of the metastable and ground-state atoms are exchanged with negligible change in polarization for either spin. In steady state, the ground-state nuclear polarization p is

$$P_g=2\langle I_z\rangle_g=\frac{\Gamma_{ex}}{\Gamma_{ex}+\gamma}P_m, \tag{4}$$

where γ is the ground-state relaxation rate, P_m is the metastable polarization, and Γ_{ex} is the metastability exchange rate per ground-state atom for the collision (3). Following the classic method of Colegrove *et al.* [3], we applied a transverse magnetic field oscillating at the nuclear Larmor frequency to see if appreciable nuclear spin polarization was generated in

the ground state by metastability exchange. We were unable to see any effect of the ground-state magnetic resonance field. Presumably, this was because the ground-state spin-relaxation rate γ of (4) is much larger than the metastability exchange rate Γ_{ex}. The ground-state relaxation comes from radiation trapping [6] and the more rapid wall relaxation in ^{129}Xe than in ^{3}He [19,20]. He atoms adsorb more weakly to walls than Xe. Also, radiation trapping is a much less serious problem for weakly ionized He plasmas, since the low-lying S states of the He atom do not radiate, but the low-lying states of Xe with $J = 1$ radiate very strongly. Previous experiments have shown effects on the spin polarization of metastable atoms due to metastability exchange collisions in metastable Xe [6,21,22]. However, a ground-state nuclear polarization has only been reported in ^{131}Xe in an electron beam experiment [22].

C. Pressure broadening

The linewidth of the hyperfine and Zeeman resonances includes a number of contributions. The spontaneous lifetime of the $1s_5$ metastable state is 43 s [23] due to quadrupole radiation for even isotopes of Xe and for the $F = 5/2$ hyperfine level of ^{129}Xe. The spontaneous lifetime is only a few seconds [23] for the $F = 3/2$ hyperfine level, since it has some admixture of the states with $F = 3/2$ and $J = 1$, which have fully allowed electric dipole transitions to the ground state. These natural lifetimes τ are so long that their contribution to the linewidth ($1/\pi\tau$ to the FWHM) will be less than 1 Hz and completely negligible compared to the observed linewidths of many tens of kHz.

Our cells contain only mTorr of Xe gas, so the atoms are not far from the ballistic regime where collisions with the walls occur more frequently than collisions with other atoms. When a metastable atom, with an excitation energy of 8.3 eV, hits the glass wall of our cell, we expect the atom to de-excite and to eject an Auger electron in the process. So the container walls should be a very potent destruction site for metastable atoms. For cells that are large enough and gas pressures that are small enough that the mean free path of a metastable Xe atom is many microwave wavelengths, the microwave resonance linewidth would be Doppler broadened to ≈6 kHz FWHM. However, our cell is small enough and the gas pressure is large enough that the mean free path is much less than a microwave wavelength, so we should be in the Dicke narrowing regime [24]. The line shapes of our microwave resonances fit a simple Lorentzian line shape very well. The fit is slightly better to a Voigt profile where a Gaussian with a width of 100 Hz is convolved with a much broader Lorentzian. With ideal Helmholtz coils, the relative magnetic field inhomogeneity over the volume of the cell is 0.13%. It contributes less than 7 kHz FWHM to the linewidth and will affect the resonances differently due to the different rates of detuning of the resonant frequencies with magnetic field. This leaves three linewidth contributions: optical pumping, power broadening from the rf or microwaves, and broadening due to collisions with other Xe atoms.

The measured FWHM linewidths for transitions between the sublevels $|3/2, m\rangle$ and $|5/2, m+\rho\rangle$ are fit to the function

$$\Delta\nu_{\mathrm{FWHM}} = \frac{1}{\pi}\sqrt{\left(\frac{1}{T_2} + aL\right)^2 + bB_1^2}. \qquad (5)$$

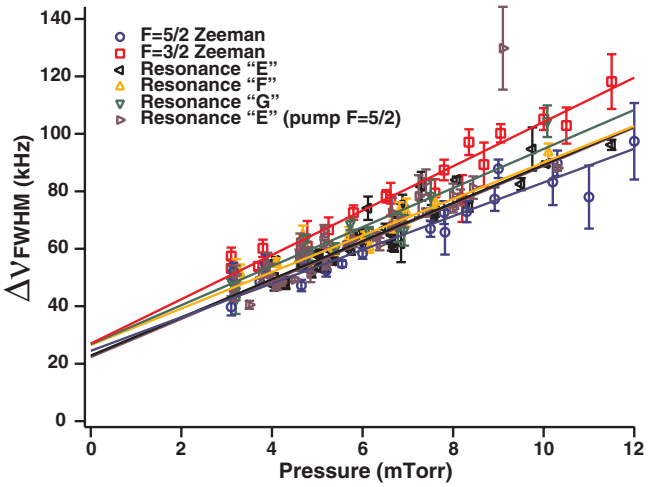

FIG. 10. (Color online) Measured linewidths $\Delta\nu_{\mathrm{FWHM}}$ for metastable ^{129}Xe hyperfine and Zeeman resonances, in kHz. (See Fig. 7 for the labeling of the resonances.) The measured pressure is in mTorr. Resonance E (pump $F = 5/2$) refers to the data acquired while pumping the $F = 5/2 \rightarrow F = 5/2$ optical transition (see Fig. 5). All other data except the $F = 5/2$ Zeeman resonance correspond to pumping the $F = 3/2 \rightarrow F = 3/2$ optical transition. The coefficients of the linear fits are given in Table II.

Here B_1 is the oscillating field amplitude and L is the laser power incident on the cell. The fitting parameters a and b are used to find the linewidths in the limit of negligible optical, microwave, or rf broadening. The residual width is characterized by T_2, the "transverse relaxation time." The linewidth of Fig. 8 is much narrower than the linewidths of the resonances in Fig. 9, because in Fig. 9, the laser intensity L was maximized to obtain the largest possible spin polarization. The laser intensity L of Fig. 8 is about two orders of magnitude smaller than that of Fig. 9.

Measurements of the pressure broadening of the resonance lines are shown in Fig. 10, which shows that the dependence of T_2 on the Xe pressure p is well described by the empirical formula

$$\frac{1}{T_2} = \eta + \kappa p, \quad \text{where} \quad \kappa = \pi\frac{d}{dp}\Delta\nu_{\mathrm{FWHM}},$$
$$\eta = \pi\,\Delta\nu_{\mathrm{FWHM}(p=0)}. \qquad (6)$$

The parameter η is the intercept and κ is the pressure-broadening coefficient of the linear fit. Each data point $\Delta\nu_{\mathrm{FWHM}}$ of Fig. 10 is the result of varying the laser intensity L and oscillating field amplitude B_1 and fitting approximately ten acquisitions to (5). $1/T_2$, which is a function of xenon pressure, is extracted from the fit to become each data point in Fig. 10. Also shown in Fig. 10 are linear fits of the extrapolated linewidths. The values for these fits are given in Table II. Many measurements were taken, and we believe the scattering is due to a combination of effects including varying levels of contamination, and perhaps different discharge conditions. Nevertheless, for the E resonances (see Fig. 7 and Table II for our labeling of the resonances) pumping both optical transitions labeled 2 and 5 in Fig. 5, both the slope and the intercept are identical, as is seen in Table II and Fig. 10. Many

factors contribute to the zero-pressure intercepts η. The most important are estimated to be diffusion to the wall, Doppler broadening, and inhomogeneities of the static magnetic field.

Although the ratio of the slopes we measure for the two Zeeman resonances with $F = 3/2$ and $F = 5/2$ is similar to those measured previously [6], the measured slopes themselves are different. The previous experiments used pure ^{129}Xe, and give, for example, a slope of 5.76 ± 0.14 kHz/mTorr for the $F = 3/2$ Zeeman resonance, while our value is 7.7 ± 0.3 kHz/mTorr. We note that previously measured pressure-broadening coefficients κ of Zeeman resonances in even isotopes of Xe have differed much more, by factors of 2–3, and this has been attributed to pressure stability issues caused by the discharge [6].

From inspection of the pressure-broadening coefficients of Table II, one can infer some characteristics of the spin interaction between metastable and ground-state Xe atoms. Many experiments have firmly established that at low magnetic fields, the depolarization of alkali-metal atoms by collisions with ground-state Xe atoms is due to a spin-rotation interaction [25]. The spin-rotation interaction is weak enough that many binary collisions are needed to fully depolarize the spin, that is, the rate coefficients κ for spin-changing collisions are many orders of magnitude smaller than those of velocity-changing collisions, which have rate coefficients of order $\kappa_{\rm vc} \approx 10^4$ s^{-1} mTorr^{-1}. The spin-depolarization coefficients of Table II are not in this regime, so a weak, spin-rotation interaction,

$$V = \gamma \mathbf{N} \cdot \mathbf{J}, \tag{7}$$

analogous to the spin-orbit interaction of alkali-metal atoms, is ruled out as the main cause of spin depolarization. In (7), $\gamma = \gamma(R)$ depends on the internuclear separation R of the colliding ground-state and metastable-state atoms. Weak, spin-rotation interactions have the selection rule $\Delta m_F = 0, \pm 1$ for the azimuthal quantum number m_F of the metastable atom. As a result of this selection rule, it requires on the order of $(2F)^2$ collisions to destroy the coherence of Zeeman resonances, since the depolarization occurs as a kind of random walk through m_F space. One or two collisions is sufficient to depolarize microwave resonances, where m_F (actually m_J) does not need to change by more than ± 1 to relax the coherence.

Two much more potent ways that collisions with ground-state Xe atoms can spin depolarize a metastable Xe atom are the spin-axis interaction and metastability exchange (see Fig. 11). Both interactions are basically of an electrostatic nature, like the spin-exchange interaction between pairs of alkali-metal atoms, and they can therefore be expected to have rate coefficients for spin depolarization comparable to rate coefficients for velocity-changing collisions. Electrostatic interactions, with their time-reversal symmetry, lead to Kramers spin doublets, so the spin-axis interaction for the metastable atom can be written as

$$V = V_2(\mathbf{J} \cdot \mathbf{n})^2 + V_4(\mathbf{J} \cdot \mathbf{n})^4 + V_6(\mathbf{J} \cdot \mathbf{n})^6. \tag{8}$$

The three potentials, $V_k = V_k(R)$ for $k = 2|m| + 2$, account for the energies of the Kramers doublets with azimuthal

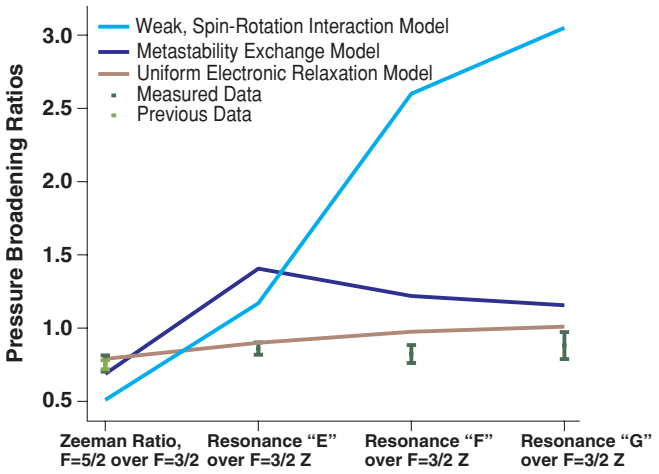

FIG. 11. (Color online) Measured and modeled pressure broadening ratios. (See Fig. 7 for the labeling of the resonances.) Measured Data, the slope of the lines from Fig. 10 and Table II; Previous Data, a measurement in pure ^{129}Xe from [6]. The modeling includes weak, spin-rotation relaxation, uniform electronic relaxation, and metastability exchange. Hyperfine resonances E and F also include contributions from $\Delta m = 0$ transitions. Curve fitting the π component of the resonance "D" (see Fig. 9) gives an amplitude and a linewidth which is comparable with the π components in resonance E and F according to the simulated population distribution (see Fig. 7). The overlap of this π component and the σ resonance E or F gives $\approx$12% change to the linewidth. A comparison of the line shapes of the overlapped resonances E and F with resonance G, which lacks an overlapping π resonance, however, shows little discrepancy. We therefore conclude that the error caused by by the overlapping π resonances is $\approx$12% or less. Our data as well as the previous data are most consistent with our uniform electronic relaxation model.

quantum numbers $|m| = 0$, 1, and 2 around the internuclear axis. The spin-axis potential accounts for the fact that the forces between the metastable Xe atom and the ground-state Xe atom will depend on how the $5p$ hole in the core of the metastable atom is oriented with respect to internuclear axis, which we specify with the unit vector $\mathbf{n} = \mathbf{R}/R$. The spin-axis interaction (8) is independent of the nuclear spin of the Xe atoms, and would be the same for all isotopes. To simplify modeling, we assume that the coefficients of the spin-axis interaction (8) are such that when collisions of all impact parameters and orientations are taken into account, the spin relaxation is "uniform"; that is, a metastable atom in a specific azimuthal state m_J before a collision is equally likely to transition to any one of the electronic sublevels with $m_J = 2, 1, 0, -1, -2$ after the collision, and the collision duration is so short that the nuclear polarization is unaffected.

For odd isotopes like ^{129}Xe, metastability exchange could cause further spin depolarization by replacing the nuclear spin of the precollision metastable Xe atom with the nuclear spin of the precollision ground-state Xe atom. As we have discussed, our experiments show no evidence for nuclear spin polarization of the ground state, so metastability exchange would be a secondary spin-depolarization mechanism.

The hyperfine spectrum seen in Fig. 9 can be fit to our model using either a combination of uniform electronic relaxation and metastability exchange or by assuming metastability exchange alone. Previous work [6] also supports a significant contribution from metastability exchange.

ACKNOWLEDGMENTS

We are grateful to Mike Souza for making the glass cells. This work was supported by the United States Defense Advanced Research Projects Agency, the Air Force Office of Scientific Research. This work was supported, in part, by US Department of Energy.

[1] F. D. Colegrove and P. A. Franken, Phys. Rev. **119**, 680 (1960).
[2] A. R. Keyser, J. A. Rice, and L. D. Schearer, J. Geophys. Res. **66**, 4163 (1961).
[3] F. D. Colegrove, L. D. Schearer, and G. K. Walters, Phys. Rev. **132**, 2561 (1963).
[4] L. D. Schearer, Phys. Rev. **180**, 83 (1969).
[5] L. D. Schearer, Phys. Lett. A **28**, 660 (1969).
[6] V. Lefèvre-Seguin and M. Leduc, J. Phys. B **10**, 2157 (1977).
[7] R. A. Zhitnikov and A. I. Okunevich, Opt. Spectrosc. (USSR) **36**, 253 (1974).
[8] L. D. Schearer, Phys. Rev. **188**, 505 (1969).
[9] C. Moore, *Atomic Energy Levels* (US Government Printing Office, Washington, DC, 1971), Vol. III.
[10] W. L. Faust and M. N. McDermott, Phys. Rev. **123**, 198 (1961).
[11] S. D. Rosner and F. M. Pipkin, Phys. Rev. A **1**, 571 (1970).
[12] J. D. Prestage, C. E. Johnson, E. A. Hinds, and F. M. J. Pichanick, Phys. Rev. A **32**, 2712 (1985).
[13] D. A. Jackson and M. C. Coulombe, Proc. R. Soc. London A **335**, 127 (1973).
[14] G. D'Amico, G. Pesce, and A. Sasso, Hyperfine Interact. **127**, 121 (2000).
[15] M. Walhout, H. J. L. Megens, A. Witte, and S. L. Rolston, Phys. Rev. A **48**, R879 (1993).
[16] M. Aymar and M. Coulombe, At. Data Nucl. Data Tables **21**, 537 (1978).
[17] SAES Getters USA, Inc., getter WHC/4-2.
[18] A. Corney, *Atomic and Laser Spectroscopy* (Clarendon Press, Oxford, UK, 1977), p. 252.
[19] X. Zeng, E. Miron, W. A. van Wijngaarden, D. Schreiber, and W. Happer, Phys. Lett. A **96**, 191 (1983).
[20] R. E. Jacob, B. Driehuys, and B. Saam, Chem. Phys. Lett. **370**, 261 (2003).
[21] T. Hadeishi and C.-H. Liu, Phys. Rev. Lett. **17**, 513 (1966).
[22] T. Hadeishi and C.-H. Liu, Phys. Rev. Lett. **19**, 211 (1967).
[23] M. Walhout, A. Witte, and S. L. Rolston, Phys. Rev. Lett. **72**, 2843 (1994).
[24] R. H. Romer and R. H. Dicke, Phys. Rev. **99**, 532 (1955).
[25] R. A. Bernheim, J. Chem. Phys. **36**, 135 (1962).